Core Diagnostics for WENDELSTEIN 7-X Steady-State Exploration Until 18 GJ*)

Matthias W. HIRSCH, Sebastian BANNMANN, Marc N. A. BEURSKENS, Christoph BIEDERMANN, Sergey BOZHENKOV, Kai-Jakob BRUNNER, Neha CHAUDHARY, Hannes DAMM, Oliver FORD, Juan GUERRERO-ARNAIZ, Gole FUCHERT, Xiang HAN[1)], Udo HÖFEL, Jia HUANG[2)], Jens KNAUER, Jean-Paul KOSCHINSKY, Andreas KRÄMER-FLECKEN[2)], Beate KURSINSKI, Andreas LANGENBERG, Samuel LAZERSON, Jens MEINEKE, Dimitry MOSEEV, Johan OOSTERBEEK, Novimir PABLANT[3)], Eckehard PASCH, Andreas PAVONE, Peter PÖLÖSKEI, Torsten RICHERT, Torsten STANGE, Matthias STEFFEN, Mathias STERN, Lilla VANÓ, Robert C. WOLF, Haoming M. XIANG[2)], Marco ZANINI, for the W7-X Team

Max-Planck-Institut für Plasmaphysik, Greifswald, Germany
[1)]*Institute of Plasma Physics, Chinese Academy of Sciences, 230031 Hefei, Anhui, People's Republic of China*
[2)]*Forschungszentrum Jülich GmbH, Institut für Energie-und Klimaforschung - Plasmaphysik, Partner of the Trilateral Euregio Cluster (TEC), 52425 Jülich, Germany*
[3)]*Princeton Plasma Physics Laboratory, US*

(Received 7 January 2022 / Accepted 5 March 2022)

This contribution provides an overview of the core diagnostics as they are required for W7-X steady-state high-density operation with a divertor and profile control. The inferred profiles then address the stellarator optimization. A particular task is the characterization of fast ion slowing down and -losses, which in a classical stellarator reactor could result in unacceptable wall loads and ultimately are deleterious for the heating efficiency. The energy dissipated during operation, 10 MW · 1800 s impacts on the technical diagnostic realization via loads to in-vessel components, quasi steady-state operation requires adequate data acquisition and control systems.

Keywords: plasma diagnostics, steady-state operation, stellarator, W7-X, profile inference, fast-ion

DOI: 10.1585/pfr.17.2406097

1. W7-X Objectives and Diagnostic Tasks

The W7-X project explores stellarator steady-state operation and develops a scenario that integrates detachment in the divertor with a reactor relevant high pressure β ~4% in the core, which should be achieved by an optimized magnetic configuration following the concept of a Helical-Axis Advanced Stellarator, HELIAS [1]. With inherently no current related Greenwald density limit in a stellarator, high-β can be realized on a high-density path. Besides the advantage of a later fusion yield $\sim n^2$, a high density increases the electron-ion coupling hence the ion heating, reduces turbulent transport by a reduced value T_e/T_i, reduces neoclassical core transport in the stellarator $1/\nu$-regime by an increased collisionality ν hence decreased diffusivity $D_{1/\nu} \sim T^{7/2}/n$ and also reduces fast ion losses by their faster slowing down. The operation density [2] is then presumably limited by edge radiation while core heating is restricted by cut-offs for the microwave beams of Electron Cyclotron Resonance Heating (ECRH) and the penetration depth of Neutral Beam Injection (NBI). In the first operational phase of W7-X high-density steady-state capable heating was shown by ECRH which for densities beyond the second harmonic x-mode (X2) cut-off was launched in ordinary mode polarization (O2) [3, 4]. This allowed safe operation at densities $< 1.5 \cdot 10^{20}\,m^{-3}$ staying well below the O2 cut-off and with T_e above the level of 2 - 3 keV as required for sufficient O2 microwave absorption.

For its second operational phase, OP2, W7-X will be equipped with a fully cooled first wall and a Carbon Fibre Composite (CFC) divertor developed for steady state operation. Successive campaigns will raise the injected energy per experiment to 18 GJ, corresponding to the project goal of a discharge duration of 1800 s at 10 MW ECRH. Interlaced high-performance phases with heating power up to 20 MW (ECRH+NBI, expected until 2027) are limited to ~10 s by the present technological conditions of NBI at W7-X. During the first operation phase peaked density profiles were a necessary ingredient to overcome Ion Tem-

author's e-mail: matthias.hirsch@ipp.mpg.de
*) This article is based on the presentation at the 30th International Toki Conference on Plasma and Fusion Research (ITC30).

perature Gradient driven turbulence (ITG) [5] which otherwise limits T_i gradients [6]. Hence, a careful mixture of heating schemes and profile shaping measures will be necessary to balance a reduction of energy transport towards its neoclassical level in a large fraction of the core while keeping sufficient turbulent particle- and impurity transport to maintain the control on the density profile and avoid accumulation.

First diagnostic operation at W7-X has been summarized in [7, 8]. This contribution now provides status and outline of core diagnostics, as they are required for a steady state high-density operation with a divertor and profile control [9]. The inferred profiles then address the aspects of stellarator optimization. A particular task is the characterization of fast ion slowing down and -losses, which in a classical stellarator reactor could result in unacceptable wall loads and ultimately are deleterious for the heating efficiency.

2. Scenario Outline

For the next operational phase, OP2 [9], the ECRH plant capable for a maximum number of 12 gyrotrons will be stepwise upgraded to approx. 14 MW by successively substituting eight units with new 1.5 MW (perspectively later 2 MW) cw-gyrotrons. This allows to maintain high-density plasmas at $1.5 \cdot 10^{20}\,\mathrm{m}^{-3}$ by O2 heating with expected central T_e = 3 - 4 keV. NBI with H ions at 55 keV can be extended to 8 sources increasing the heating power to 9.5 MW (15 MW in D). Under present technological conditions NBI operation is limited to phases < 10 s every 5 to 10 minutes determined by the Titanium-pumps, extraction magnet and uncooled ion dump. Ion Cyclotron Resonance Heating (ICRH) with 2 MW at 25 MHz can be operated for 10 s every 10 minutes interacting in the 3He minority scheme (with > 0.1% He). It is considered as a fast particle source rather than a heating system and provides fast ion energies > 100 keV. At the *begin* of OP2 about 9 MW ECRH *or* 7 MW NBI *or* 12.5 MW in combined mode ECRH+NBI will be available only, limited by the presently installed transformers.

As of exhaust the cooled CFC divertors are expected to cope with 10 MW in attached mode under steady state conditions. Higher power loads must be temporary (e.g. during phases with NBI) or require detachment [10]. The envisaged timeline is a stepwise increase of plasma energy in a series of annual campaigns with steps such as 1 GJ, 2 GJ, 6 GJ and finally 18 GJ followed by a longer (several years) shutdown for replacement of carbon as divertor- and in-vessel material. Deuterium operation is required to investigate the isotope effect on transport and on possible improved confinement modes, to increase the available NBI heating power and for the use of neutron emission as plasma diagnostics. A two year preparation phase is expected before first D-operation; a schedule has not yet been decided. We note when switching NBI to D-operation at 60 keV the higher port through power (8 sources then launch 20 MW) is partially compensated by higher charge exchange losses.

W7-X has been optimized for a reactor relevant working point at $\langle\beta\rangle$ = 4% hence the success of optimization criteria such as reduced neoclassical transport or an improved fast ion confinement in the plasma core comes with increasing β. Extrapolating global confinement from the International Stellarator Scaling ISS05 while assuming τ_E/τ_{ISS} = 1.4, as observed for the best W7-X confinement cases obtained temporarily after pellet injection in the first operation phase [7] shows, that at densities $1.5 \cdot 10^{20}\,\mathrm{m}^{-3}$ a pressure $\langle\beta\rangle$ = 4% requires a power of 30 - 40 MW. The same β can be achieved already with 20 MW at reduced magnetic field, B = 1.7 T, with the available 140 GHz gyrotrons heating the 3rd harmonic. In this case densities can be only $1.0 \cdot 10^{20}\,\mathrm{m}^{-3}$ as higher densities are already prone of the Sudo density limit [2]. The lower magnetic field also reduces mechanical forces in the coil system hence broadens the accessible configuration space by minimizing mechanical load cycles. Therefore such a scenario and a related plasma start-up will be developed as one goal of the next operation.

3. Requirements for Steady State Diagnostics

Observation geometries in the modular stellarator are restricted by port placement in the remaining coil interspaces. For example in W7-X there is only one type of (narrow) opposite ports available that allows for a sightline passing the plasma center. An advantage is the large aspect ratio which allows for some ports from the inboard side of the torus as well. In total W7-X has ~250 diagnostic ports widely symmetric in 5 modules with largest port aperture of 100 cm · 40 cm and a typical distance of ~1.8 m between aperture to the plasma vessel and port lid. Respective plugins must cope with port movements by changes in the magnetic configuration and changing loads (pump-down, cooldown, ...) resulting in respective tolerances that reduce the usable port aperture and must be taken into account for diagnostic design. The helical axis and toroidally varying shape of the HELIAS confinement region require oblique sightline geometries aside the two types of symmetry planes. The high stiffness of the magnetic configuration versus β, a result of the HELIAS optimization that minimizes internal currents, allows to design sightlines that can cope with a variety of configurations and plasma scenarios even for plasma start up, the latter in contrast to a tokamak. Therefore the exploration of the configuration space in upcoming OP2, ultimately the selection of a candidate configuration for an integrated high-performance scenario for which the W-divertor can be optimized, has no severe impact on core diagnostic design - in obvious contrast to diagnostics at the plasma edge. However, around the last closed flux surface, diagnostic mapping for crosscheck and

itegrated data analysis may become challenging due to the presence of magnetic islands modified by a finite pressure gradient and finite bootstrap current there.

Steady state operation with 100 kW/m^2 design heat load reaching thermal equilibrium for all in-vessel components requires their active cooling. In total W7-X includes ~600 cooling circuits which have to be qualified with 40 bar @ 150°C baking temperature. For design heating energy stages have been defined that assume a series of 30 shorter preparative pulses 10 MW @ 10 s with dwell times between followed by a single 10 MW pulse with up to 30 minutes at the end of the day. Alternatively a maximum heating energy of 24 MW @ 30 s is used as design specification.

Unabsorbed ECRH power, multiply reflected and scattered from the stainless steel- or graphite wall components builds a nearly isotropic microwave stray-radiation background. Its toroidally asymmetric power flux density reaches ~50 kW/m^2 in particular with steady state O2 heating where single pass absorption is 80% only [11]. This background - like a microwave photon gas - creeps in subvolumes of diagnostic arrangements and the deposit energy accumulates in all microwave absorbing components such as isolations and ceramics there which therefore have to be shielded or particularly cooled [12]. In endangered locations such as near detectors or at the cryopumps dedicated microwave absorbing ceramic layers on actively cooled metal structures may dilute this background [13]. Diagnostic windows can be coated by microwave reflecting Indium Tin Oxide-layers (ITO) that reflect microwaves but are transparent in the visible, a solution which is, however, not applicable in the IR [14]. In the latter case microwave stray radiation may leave the torus and windows and diagnostic components outside them must be monitored. To qualify diagnostics and other in-vessel components, a dedicated program has been set up with the Microwave STray RAdiation Launch Facility MISTRAL [12] which allows to test even complete lager port plugins over 30 min in an isotropic microwave background of up to 50 kW/m^2 with power provided from one of the 140 GHz long-pulse gyrotrons.

The variety of diagnostic frontends ranges from open ports with cooled liners (e.g. for pellet- or diagnostic beam injection) to fully cooled stainless steel plugins and even to evacuated immersion tubes with windows closer to the plasma. Diagnostics should use mirrors as first optical elements, with vacuum windows ideally retracted and cooled at their edges. Cooled shutters allow to open optical diagnostics on demand only such as for active Charge Exchange Resonance Spectroscopy, CXRS, which is open only when the neutral beam is on. Movable parts are simple push and pull avoiding sliding mechanics. Complex 3D shaped frontend geometries with minimized aperture and integrated cooling have been manufactured by qualified Selective Laser Melting, SLM. An example of a highly integrated plugin with a SS port shield for cw operation

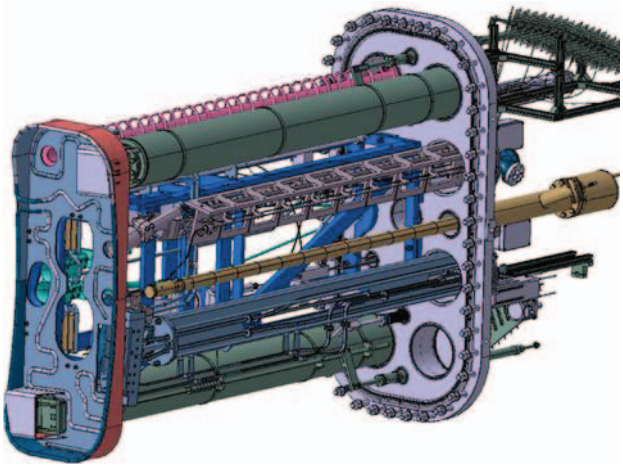

Fig. 1 Drawing of a diagnostic plugin for a 1000 mm × 40 mm aperture port integrating more than ten diagnostics such as poloidal correlation- and Doppler reflectometry, the latter one with steerable beam direction, correlation ECE, a wide angle sniffer probe for microwave stray radiation, a manometer, two immersion tubes with movable mirrors/shutters for active and passive spectroscopy, SOL coherence imaging, and an Alkali diagnostic beam right along the port axis (the latter not indicated).

electro-plated at its plasma distant side with ~3 mm Cu to improve heat conduction to the cooling pipes there is shown in Fig. 1.

The development towards long discharges requires to cope with possible thermal drifts in calibrations or accumulated changes in transmission or reflection of first optical components. For long pulse operation in-situ recalibration or drift control must be qualified in some cases possibly arranged in dedicated calibration segments of the long pulse experiment later. Finally the effort necessary for cw-DAQ, the identification of component failure during operation, diagnostic synchronization and control in predefined discharge segments is often underestimated.

In contrast to these technical specifications the physics demands to core diagnostics are widely unaffected by the discharge length and more determined by the 10 to 20 s high-performance phases defined by NBI availability. For some of the diagnostics the long interlaced high-power ECRH phases may even be used for recovery, crossceck and interlaced data storage.

4. Core Diagnostics for Operation and Control

Autonomous control of a steady-state high performance plasma, next to the mandatory qualitative understanding of the related physics processes, requires reliable diagnostic signals, a control system and actuators such as the flexible heating systems or various fuelling capabilities for example. In a stellarator there is, however, no need for fast disruption control. For W7-X tracking of the following core parameters is prepared as a first step:

- line averaged density measurements and related feedback density control have been established reliably already in OP1 from a single channel Dispersion Interferometer (DI) using real time phase demodulation on a Field Programmable Gate Array, FPGA [15]. After the system had been set up practically no discharge has been lost even under highly perturbed conditions such as pellet injection or strong thermal plasma crashes [16]. As a backup for feedback control the central channel of the multichannel interferometer is being prepared.

- the peaking of density profiles is considered as a control parameter, as high-T_i scenarios seem to rely on peaked density profiles providing finite density gradients around mid radius as an ingredient for ITG mitigation [5]. For this purpose a multichannel interferometer is being prepared for continuously tracking moments of the density profile shape such as the peaking factor. Actuators on the density profile in such improved scenarii could be deep fuelling by pellets or NBI versus edge fuelling measures in combination with divertor pumping and possible T_e or n_e profile shaping by off-axis ECRH.

- a proxy for the edge "upstream" density as a main control parameter for divertor operation is provided continuously by the edge channel of the multichannel interferometer. For geometrical reasons its innermost touched flux surface is not further out than $\rho \sim 0.95$.

- a core electron temperature exceeding 2 - 3 keV is required for sufficient O2 ECRH absorption in high-density discharges. With lower T_e the O2 absorption degrades and the density must be reduced or heating power added. As standard X2 ECE is hampered by cut-off the optically grey 3rd harmonics has been studied with a broadband Michelson interferometer [17, 18]. For tracking T_e under these conditions and provide a continuous control signal an X3 radiometer is being prepared eventually applying forward analysis and correction factors for the reduced optical thickness [19].

- real time analysis of Thomson scattering is presently being explored as an option to supplement T_e and n_e profile tracking in high density plasmas.

- finally a continuous measurement of the agreed neutron rate and neutron budged in later D-plasmas of W7-X is requested from the authorities. For this purpose three neutron monitors with five detectors of different overlapping sensitivity each allow to measure neutron fluxes varying over more than five orders of magnitude. In-situ calibration is achievd with a neutron source moved around the plasma axis [20].

The diagnostics that are directly related to operation and safety of the heating systems themselves are beyond the scope of this paper. For ECRH, next to beam transmission, they measure the toroidal distribution of the isotropic microwave stray radiation background by wide angle microwave sniffer probes [11, 12, 21]. For NBI wall loads from direct shinethrough are monitored. Finally reflectometry probing the gap between the plasma edge and the ICRH antenna supports the optimization of RF-plasma coupling but also completes the overall density information if ICRH is off.

5. Core Profile Diagnostics

Objective are routinely available qualified core profiles of electron density $n_e(r)$, electron- and ion-temperature $T_e(r)$ and $T_i(r)$, the radial electric field $E_r(r)$ and a contribution to profiles of Z_{eff} and the density of individual impurities. The provision and assessment of large data-streams of reliably calibrated and qualified profiles in due time is challenging on the DAQ and software side albeit seemingly technically straightforward. Post-processing and integrated data analysis is required at different levels of complexity hence delivery time: Soon after or even during the experiment key quantities must be provided taking into account only a minimum of necessary interdependencies or even a first educated guess. The availability of further evaluated data or recalibrations requires reprocessing to a versionized profile information taking into account more interdependencies such as the actual best knowledge on the plasma equilibrium for example. Finally fully integrated analyses using Bayesian principles are available on demand [22, 23]. Data handling strategies such as neuronal networks for often used complex interdependencies are also being explored [23].

Thomson scattering providing T_e and n_e profiles is the workhorse of profile analysis [24]. Three lasers with ~1.8 J per pulse can be staggered to provide nearly 10 ms time resolution. Two observation optics cover a total of presently 42 volumes on the inboard- and outboard side of the plasma by means of 20 polychromators with 5 spectral channels each. An event-synchronized 18 pulse "burst" sequence within an ~1.5 ms short interval with full laser energy but repetition then reduced to 5 Hz can be realized for fast events such as the density evolution after pellet injection [25]. In preparation of long-pulse operation an automated laser beam position control is presently implemented to cope with geometrical drifts of the necessary long pathways of more than 30 m.

Density profiles in OP1 derived from absolute intensity calibration by Raman scattering at low nitrogen pressure in the vessel suffered from drifts resulting possibly from observation window coating and from laser-beam pointing scatter [26]. As for each individual pulse, the laser axis on the Brewster windows is tracked by cameras the concept of a beam-position dependent Raman calibration is presently being explored [27]. In-situ spectral calibration including the effect of the vacuum window is implemented using both Raman- and Rayleigh scattering with a tunable source (an Optical Parametric Oscillator, OPO, pumped by a Nd:YAG) launched along the same sightline [28]. This allows an improved spectral calibration due to better resolution of the filter edges with the narrow OPO line width. The absolute calibration of all spectral chan-

nels improves as the scattered light of the OPO provides a realistic light source with a realistic image to the detector diodes instead of an isotropic illuminated white surface used so far. Moreover, despite a pulse energy of the OPO that is ~200 times smaller than the Nd:YAG, the strong Rayleigh signal allows in-situ calibration at a lower N_2 gas pressure. This has operational advantages for more frequent calibrations as mechanical load changes of the W7-X vessel when changing to a finite N_2 pressure can be reduced. Despite promising first results with the OPO [29], the method needs further improvement by a better suppression of false-light from the entrance window to achieve an improved signal-to-background level. Respective in-vessel stray light absorbers have been installed.

Two-wavelength Thomson scattering has been prepared for the next campaign with a second longer wavelength YAG-laser (λ = 1319 nm) launched along the same mirrors and sightline [30]. Using the same set of observation filters this gives access to higher electron temperatures and evaluates an option for in-situ cross calibration of the T_e-measurement.

The multi-sightline Dispersion Interferometer yields redundancy for density control by its core channel, provides a continuous proxy for the upstream density by its edge channel and allows to track the profile shape in view of density profile shape control. The four channel system under development will provide a density profile peaking factor. Most critical component are high-heatload Corner Cube Retoreflectors (CCR) integrated and cooled via the first wall tiles which are an unavoidable consequence of the available port geometry [31]. A maximum of 10 channels is geometrically possible by the available retroreflector slots in the high-heatload tiles of the wall. Tests of reflectors, which had been installed already during OP1.2, did not indicate degradation for the relevant 10 µm / 5 µm wavelengths. The DI interferometers also serve as testbed for DEMO preparation studies and support the ITER start-up Dispersion Interferometer (DIP) [32]. This includes testing of improved high-efficiency frequency doubling technology by GaAs/AlGaAs-heterostructures and higher modulation frequencies using either acousto-optical or electro-optical modulators. The latter allows to track Alfven modes until frequencies of several MHz in preparation of studies of the fast ion loss dynamics. A test DI system based on a Nd:YAG which requires much less laser power and may use standard doubler techniques with higher doubling efficiency is also being prepared. It could solve stability issues with the high power CO_2-laser the DIs presently use.

Density profile inference in the deep core may be addressed by an integrated Bayesian analysis combining Thomson scattering with multi-sightline interferometry which provide complementary information with respect to temporal and spatial resolution. In the first campaign of W7-X a weaker information on the edge density could be tolerated as pedestal physics had not yet played a major role. High resolution density profiles right inside the last closed flux surface besides their own value, e.g. for neutron penetration and pedestal physics are required for the localization of the various Doppler- and correlation reflectometer measurements providing e.g. the poloidal edge rotation and the separatrix position from the velocity shear layer. Options for edge density measurements aside the edge channel of the interferometer are the already existing sodium beam [33], an improved S/N ratio of edge Thomson channels (an edge resolution down to 0.5 cm volumes is geometrically possible) and density profile reflectometry which will use the X-mode V- and W-band reflectometers integrated in the ICRH antenna [34]. A particular complexity of a combined edge density analysis in island divertor configurations is, that the individual sightlines cross edge islands at different locations with respect to their X- an O-point.

Electron temperature profile inference: Core electron temperature measurements are provided by Thomson scattering, Electron Cyclotron Emission (ECE) and the X-ray imaging diagnostics which uses the ratio of Ar-impurity emission lines. An integrated T_e-profile analysis will be prepared.

The 140 GHz X2 ECE radiometer employs 32 channels probing the full plasma cross section with optimized spatial resolution obtained by small emission volumes that are realized with an in-vessel Gaussian optics. Gyrotron stray radiation is blocked by a notch filter [35]. Absolute calibration of the measured radiation temperature is obtained with a hot-cold source using Bayesian analysis [36]. It requires high linearity and robustness versus drifts of the system components - the latter a possible issue for long discharges, where optionally fast calibration segments switching to a calibrated noise source could be interlaced. For higher radial resolution a 16 channel "zoom" system is available which covers a frequency range of 4 GHz corresponding to 4 to 8 cm in real space that can be tuned to a suitable position along the sightline [37]. The inference of a local electron temperature from the measured radiation temperature spectrum is complex as it includes the 3D plasma equilibrium (provided by VMEC code [38]) but also beam refraction and radiation transport modelling (provided by the TRAVIS code [39]) such that for many conditions an integrated forward analysis is necessary. For operation at B-field reduced to 1.7 T with the 140 GHz gyrotrons heating in the 3rd EC-harmonics the radiometer inherently measures the optically grey X3 emission which requires forward modelling to derive the T_e-profile [19]. ECE due to its continuity and the high temporal resolution also adresses the ECRH power deposition and dynamic electron heat transport: This includes ECRH induced heatwaves as well as any propagating temperature perturbation such as a consequence of pellet injection or of intrinsic transport events, either in the core or ELM-like events at the plasma edge [40]. ECE also provides the radial localization and possibly radial mode structure of MHD activity

such as Alfven waves, sawtooth crashes and plasma terminating events [16].

Two imaging X-ray spectrometers are operated which observe the line integrated emission of heavy impurities introduced into the plasma for diagnostic purposes. Radiation is collected along a fan of sightlines covering a large area of the plasma cross section and spectrally dispersed by means of Bragg reflection at a spherically bent crystal onto a large area 2D detector. For proper signal levels, only trace amounts of impurity densities are required. The X-ray Imaging Camera System (XICS) [41, 42], jointly operated with the Princeton Plasma Physics Laboratory, uses Ar^+ emission lines to measure routinely T_i (from line broadening), T_e (from a ratio of Ar lines) and E_r (from their Doppler shift) along these sightlines. For the upcoming campaigns Doppler measurements have been improved by an ex-vessel x-ray calibration source. Radial profiles are available in the core and gradient region but unavailable in the edge (due to minimum T_e needed to ionize Ar to the required charge states). They are determined from the line integrated signals through the use of tomographic inversions based on a known equilibrium. In the central core region the accuracy of the inverted profiles depends on both available signal level as well as the hollowness of the emissivity profiles. A fast inversion process using neuronal network has been implemented to provide continuously core Ti data during experiments [23]. The High-Resolution X-ray Imaging Spectrometer, HR-XIS [41,43], measures emission from several highly ionized states of various heavy impurities (Si8+, Ar17+, Ti21+, Fe25+, Cu28+, Mo33+), monitoring impurity concentrations with high sensitivity ($n_Z/n_e \sim 5e^{-5}$) and their temporal behavior e.g. after their injection via Laser Blow-Off. The different impurity lines are selected by flipping the spectrometer crystals. In preparation of a full metall device Tungsten transport can be investigated via W44+, and the higher states W64+ to W62+ using appropriate crystals.

Visible Core Spectroscopy is arranged around the heating beams with four immersion tubes desigend to cope with steady-state conditions and allows 257 sightlines, of which a bunch of 176 are presently routed to 7 effective spectrometers in the laboratory outside the torus hall. Obtained are active Charge Exchange Resonance Spectroscopy (CXRS) measurements and the Beam Emission Spectroscopy (BES) around the H-alpha line that provide the total beam power and shinethrough, but also the beam particle fueling profile, the He/H ratio and the fast ion density distribution via Fast Ion D-alpha (FIDA) measurements. The good S/N ratio allows active CXRS even during ~10 ms NBI blips in otherwise ECR heated discharges. T_i-profiles are obtained from Doppler broadening of intrinsic Carbon and Boron impurity lines. Other impurities, e.g. those from impurity injection or appearing as a result of seeding (O, Ar, Fe, Ne, N), are available. The fact that the same volume is probed under different angles allows to derive profiles of the perpendicular flows hence E_r, the parallel flow velocty and as well as the impurity concentrations. The active spectroscopy is supplemented by an additional passive system with line integrated measurements from the plasma edge (r/a > 0.8), providing T_i, E_r, Z_{eff} or neutral density measurements from electron excitation and charge exchange with edge neutrals.

The Ti profiles derived from CXRS impurity lines are in relatively good agreement with the continuous measurements from X-ray imaging at Ar. Preliminary systematic differences which showed ~0.3 keV higher values in the X-ray system could be reduced to within the expected systematic error of each diagnostic (~0.1 keV). A integrated Bayesian T_i analysis and a real time XICS T_i profile inference using neural networks are in preparation.

Z_{eff} profiles are derived by Bayesian forward analysis [44] using spectrometers directly dedicated to Bremsstrahlung measurements and supplemented by the core spectroscopy. Calibrated Bremsstrahlung profiles also may be derived from the background of the Thomson channels, which, however, has not yet been systematically evaluated in comparison to dedicated continuous spectrometers.

Magnetic-field- and iota-profile measurements are being evaluated: The unexpectedly good Beam Emission Spectroscopy signals around the H-alpha line allowed to measure the splitting of σ- and π- Motional Stark Effect (MSE) spectral components from which the local magnetic field value may be derived. A dedicated system is presently under study.

6. Fast Ion Diagnostics

Alpha particle confinement is a particular issue in a helical reactor where losses may hamper a burning plasma and the narrow loss cones of escaping fast ions may lead to inacceptable highly localized wall loads. The HELIAS configuration of W7-X is therefore optimized for improved fast particle confinement in the inner core at $\beta \sim 4\%$. In the absence of alpha particles in W7-X fast hydrogen ions (FI) from NBI and ICRH serve as a proxy for alpha particles with similar ratio of gyroradius to minor radius, ρ/a.

Following Ascot code calculations FI wall loads are expected mostly in the coil ripple of the edge magnetic field stength and at a few protuding components [45]. In OP1 IR-camera measurements that allowed to subtract IR-patterns during and after an NBI blip were limited to individual areas around the divertor [45]. The visible in-vessel camera observation system is hampered by edge plasma emission hence limited to the afterglow and thus sensible to very high heatloads only. Therefore a dedicated IR-observation system for FI wall loads is presently being designed to monitor at least selected endangered locations. A full coverage of the inner vessel with such a system is out of the scope of this project, which therefore relies on modelling cross calibrated by individual measurements at some locations. Results will impact on the decision to upgrade the NBI system to eight sources or to prolong its

pulse length.

For a sound assessment of the improved central core confinement of fast ions - crucial for a next step device - it must be proven that with the proper configuration selected and with increasing β (values between 2 and 4%) the phase space of fast hydrogen particles changes beneficially as predicted by the codes.

The *experimental issue* thereby is that with the β increase and the developing profiles of density, temperature and radial electric field all variables of the phase space, the birth profile, the slowing down and hence the wall load intrinsically change. The *diagnostic issue* is that the idealized goal of such a "phase space tomography" must be approximated with diagnostics that probe a section of this phase space only as given by their diagnostic principles and in particular their restricted diagnostic access geometries. The task is fully 3D already in real space, as due to the toroidally localized FI birth at the heating sources neither toroidal- nor stellarator symmetry hold. Finally, dynamic losses due to FI driven mode activity need to be quantified and ultimately controlled as well.

Hence, this fast ion project heavily relies on modelling as a parenthesis of the available diagnostic information [45, 46]. As one step predictive modelling of diagnostic signals is required to identify the proper set of diagnostics and their locations that allow to distinguish those changes in phase space that have been identified as features that indicate improved FI core confinement. Moreover, fast ion diagnostics in most cases still have to be developed, qualified and integrated:

The birth profile of FI resulting from NBI is calculated from beam deposition calculations with BEAMS3D [46] and measured by the Beam Emission Spectroscopy.

Fast Ion slowing down can be followed with a number of diagnostics, all of them providing a very localized glance to the phase space:

Collective Thomson Scattering (CTS) using a gyrotron beam and dedicated microwave optics measures the distribution function of thermal and fast ions. First tests with a 140 GHz beam in OP1 were hampered by a strong ECE background. A 175 GHz gyrotron is being prepared to allow CTS measurements aside this background [47,48].

Fast Ion H- or D-alpha (FIDA) emission resulting from charge exchange of beam neutrals with fast ions adds a broad background structure around the strong hydrogen alpha line of the Beam Emission Spectroscopy spectrum. The active FIDA signal from interaction with neutrals along the beam is overlayed with a toroidally and poloidally asymmetric FIDA background resulting from interaction of FI with edge neutrals. It is presently studied if additional FIDA lines-of-sight from spacially distributed small optical units integrated in first wall elements could disentangle the required information of the FI distribution [49].

Ion Cyclotron Emission spectroscopy (ICE) has been tested in OP1 with a detector prototype integrated in an wall observation camera plugin. For OP2 polarization dependent measurements will be possible with a 4-sensor array attached to the plugin for CTS observation optics or using the ICRH antenna as another receiver [50].

Charge Exchange Neutral Particle Analyzers (CX-NPA) measure the escaping charge exchange neutrals resulting from interaction of a neutral particle beam and hence provide the slowing down distribution of the fast particles in addition to the thermal ion energy distribution. In W7X for geometrical reasons active CX-NPA is not possible at the heating beams and predictive analyses for a dedicated diagnostic beam showed that magnetic configurations with varying FI confinement lead to only small signal differences for the accessible observation geometries there [51]. No further dedicated activities are presently assumed for this project.

A pinhole view to the phase space of escaping fast ions at individual locations outside the plasma is provided by angle- and energy-selective Fast Ion Loss Detectors (FILD). Using a slit or a diaphragm in front of the detector pitch angles and gyroradius hence energy can be discriminated. The good temporal resolution allows to identify FI-losses associated with mode activity. In OP1 a first Faraday cup detector successfully operated together with NIFS, Japan, has been attached to the Multi-Purpose-Manipulator (MPM) and demonstrated angular and energy resolution with its pinhole-like aperture and a 6 pixel detector [52]. A more advanced FILD with a slit and a scintillating detector plate behind observed with a camera via fibres is presently under design together with the Priceton Plasma Physics Laboratory, US. For a spatially wider analysis of fast ions escaping to various endangered components of the wall thin film layered Faraday cup detectors have been developed [42]. By varying the thickness of the isolating top layers these in-tile FILD provide some spectral but no angular resolution. The detectors will integrated in tiles of the first wall; predictive optimization of required detector placements has already been done [53]. A prototype integrated in a graphite wall-tile mock-up attached to a movable plugin has already been installed for the next experiments.

Acknowledgements

This work has been carried out within the framework of the EUROfusion Consortium and has received funding from the Euratom research and training programme 2014-2018 and 2019-2020 under grant agreement No 633053. The views and opinions expressed herein do not necessarily reflect those of the European Commission.

[1] G. Grieger *et al.*, Fusion Eng. Des. **25**, 73 (1994).
[2] G. Fuchert *et al.*, Nucl. Fusion **60**, 036020 (2020).
[3] R.C. Wolf *et al.*, Plasma Phys. Control. Fusion **61**, 014037 (2019).
[4] H.P. Laqua *et al.,* Nucl. Fusion **61,** 106005 (2021).

[5] S.A. Bozhenkov *et al.*, Nucl. Fusion **60**, 066011D (2020).
[6] M.N.A. Beurskens *et al.*, Nucl. Fusion **61**, 116072 (2021).
[7] M. Krychowiak *et al.*, Rev. Sci. Instrum. **87**, 11D304 (2016).
[8] R. König *et al.*, J. Instrum. **10**, P10005 (2015).
[9] In summer 2020 a Temporary Working Group developed a proposal for the strategy of W7-X towards an assessment on the rector capability of the underlying HELIAS configuration as requested from the EUROfusion program for soon after 2030 as basis of a next device. The final report "W7-X strategy 2030" 1-YLF-T0000.0 has been submitted to and has been approved by the scientific board of directors.
[10] D. Zhang *et al.*, Nucl. Fusion **61**, 126002 (2021).
[11] D. Moseev *et al.*, Nucl. Fusion **57**, 036013 (2017).
[12] M. Hirsch *et al.*, AIP Conf. Proc. **1612**, 39 (2014).
[13] D. Zhang *et al.*, 38th EPS Conference on Plasma Physics (2011), P5.056.
[14] J.W. Oosterbeek *et al.*, 2021, Stray radiation exposure of vacuum windows in the MISTRAL facility, to be submitted to Fusion Eng. Des.
[15] K.J. Brunner *et al.*, J. Instrum. **13**, P09002 (2018).
[16] M. Zanini *et al.*, Nucl. Fusion **60**, 10602 (2020).
[17] J.W. Oosterbeek *et al.*, Fusion Eng. Des. **146**, A 959 (2021).
[18] N. Chaudhary *et al.*, J. Instrum. **15**, P09024 (2020).
[19] C. Chaudhary *et al.*, *Investigation of optically grey electron cyclotron harmonics in Wendelstein 7-X*. Doctoral thesis, TU Berlin, http://dx.doi.org/10.14279/depositonce-12630., submitted to Plasma Phys. Control. Fusion (2021).
[20] W. Schneider *et al.*, J. Instrum. **7**, C03025 (2002).
[21] F. Gandini *et al.*, Fusion Eng. Des. **56-57**, 975 (2001).
[22] J. Svensson and A. Werner, Large Scale Bayesian Data Analysis for Nuclear Fusion Experiments, In: 2007 IEEE International Symposium on Intelligent Signal Processing (3rd - 5th Oct. 2007). Alcalá de Henares, Madrid, Spain, Oct. 2007.
[23] A. Pavone *et al.*, Plasma Phys. Control. Fusion **61**, 075012 (2019).
[24] E. Pasch *et al.*, Rev. Sci. Instrum. **87**, 11E729 (2016).
[25] H. Damm *et al.*, J. Instrum. **14**, C09037 (2019).
[26] S. Bozhenkov *et al.*, J. Instrum. **12**, P10004 (2017).
[27] G. Fuchert *et al.*, submitted to J. Instrum. (2021).
[28] S. Bozhenkov *et al.*, Rev. Sci. Instrum. **90**, 033505 (2019).
[29] E.R. Scott *et al.*, J. Instrum. **14**, C10033 (2019).
[30] E. Pasch *et al.*, Rev. Sci. Instrum. **89**, 10C115 (2018).
[31] X.B. Peng *et al.*, Fusion Eng. Des. **89**, 318 (2014).
[32] K.J. Brunner *et al.*, Design considerations of the European DEMO's IR-interferometer/polarimeter based on TRAVIS simulations, submitted to J. Instrum. as Proceedings of the International Conference on Diagnostics for Fusion Reactors, Varenna 2021.
[33] S. Zoletnik *et al.*, Rev. Sci. Instrum. **89**, 10D107 (2018).
[34] X. Han *et al.*, Design and characterization of a dual-band X-mode reflectometer for the electron density profile measurement at the ICRH antenna on Wendelstein 7-X to be submitted to Rev. Sci. Instrum. (2022).
[35] M. Hirsch *et al.*, EPJ Web of Conferences **203**, 03007 (2019).
[36] U. Höfel *et al.*, Rev. Sci. Instrum. **90**, 043502 (2019).
[37] C. Fuchs and H.-J. Hartfuss, Rev. Sci. Instrum. **72**, 382 (2001).
[38] S.P. Hirshman and J.C. Whitson, Phys. Fluids **26**, 3553 (1983).
[39] N.B. Marushchenko *et al.*, Comput. Phys. Commun. **185**, 165, ISSN 0010-4655 (2014).
[40] M. Hirsch *et al.*, 46th EPS Conference on Plasma Physics P2.1054 (2019).
[41] A. Langenberg *et al.*, Rev. Sci. Instrum. **89**, 10G101 (2018).
[42] N.A. Pablant *et al.*, Phys. Plasmas **25**, 022508 (2018).
[43] A. Langenberg *et al.*, Phys. Plasmas **27**, 052510 (2020).
[44] S. Kwak *et al.*, Rev. Sci. Instrum. **92** (2021).
[45] S. Äkäslompolo *et al.*, Nucl. Fusion **58**, 082010 (2018).
[46] S. Lazerson *et al.*, Nucl. Fusion **60**, 076020 (2020).
[47] D. Moseev *et al.*, Rev. Sci. Instrum. **90**, 023501 (2019).
[48] D. Moseev *et al.*, J. Instrum. **15**, C0503 (2020).
[49] P. Poloskei *et al.*, Experimental characterization of the active and passive fast-ion H-alpha emission in W7-X using FIDASIM, submitted to Nucl. Fusion (2021).
[50] D. Moseev *et al.*, Rev. Sci. Instrum. **92**, 033546 (2021).
[51] S. Bannmann *et al.*, Feasibility of neutral particle analysis for fast-ion measurements at W7-X, submitted to J. Instrum. (2021).
[52] K. Ogawa *et al.*, J. Instrum. **14**, C09021 (2019).
[53] D. Kulla, S. Lazerson *et al.*, Placement of a fast ion loss detector array for neutral beam injected particles in Wendelstein 7-X, accepted for publication Plasma Phys. Control. Fusion as 103670.R1 (2021).